

# One-pot preparation of three-dimensional macroporous phosphomolybdic acid-MoS<sub>2</sub>-reduced graphene oxide hybrid for electrochemical detection of nitrite

Hui Xu<sup>1</sup>, Guangran Ma<sup>1,2</sup>, Meijuan Wu<sup>1</sup>, Xia Peng<sup>1</sup>, Lin Wang<sup>1</sup>, Fugang Xu<sup>1,\*</sup>

<sup>1</sup> College of Chemistry and Chemical Engineering, Jiangxi Normal University, Nanchang 330022, China

<sup>2</sup> Analytical and Testing Center of Jiangxi Normal University, Nanchang, 330022, China

\*E-mail: [fgxu@jxnu.edu.cn](mailto:fgxu@jxnu.edu.cn)

Received: 12 April 2019 / Accepted: 5 June 2019 / Published: 30 June 2019

---

In this study, a new hybrid PMA-MoS<sub>2</sub>-rGO composed of phosphomolybdic acid (PMA), MoS<sub>2</sub>, and reduced graphene oxide (rGO) was prepared for sensitive electrochemical detection of nitrite. The hybrid was prepared by a facile one-pot hydrothermal reaction, and PMA was introduced as active species for catalytic oxidation of nitrite and Mo source of MoS<sub>2</sub>. The structure and component of the product were characterized by SEM, Raman and EDS, and its catalysis toward nitrite oxidation was investigated by several electrochemical methods. The results revealed the hybrid composed of flower-sphere-like MoS<sub>2</sub> interwind with rGO sheet while PMA doped in them, forming a three-dimensional porous structure. The MoS<sub>2</sub> flower-sphere greatly reduced the aggregation of rGO and increased active surface area of the hybrid. Introducing rGO improved the conductivity and greatly enhanced the catalytic current. PMA played a dominate role in catalytic oxidation of nitrite. Owing to these synergy interactions, the hybrid exhibited greatly enhanced catalysis for nitrite oxidation than MoS<sub>2</sub> or PMA-MoS<sub>2</sub>. The hybrid was used for fabricating a nitrite electrochemical sensor, which showed a linear rang of 0.5 μM to 8000 μM and a LOD of 0.2 μM (S/N=3). The sensor also showed good selectivity and stability with satisfactory recoveries for real sample test. The PMA-MoS<sub>2</sub>-rGO hybrid with easy preparation, porous structure, high stability and good catalysis holds great potential in environmental monitoring, chemical analysis, and so on.

---

**Keywords:** MoS<sub>2</sub>, polyoxometalates, nitrite, graphene, nanohybrid, electrocatalysis.

## 1. INTRODUCTION

Nitrite prevails in our life as industry agents and metabolite of nitrogenous species. However, the excessive uptake of nitrite cause side effect on human health [1-3]. Therefore, accurate monitoring nitrite

level is of great importance. Although many methods have developed for nitrite sensing, electrochemical sensors have received considerable attentions owing to their merits of high sensitivity, low cost and easy miniaturization. Generally, nanomaterials modified electrode are widely used to improve the sensitivity, selectivity, and reduce over-potential and electrode fouling [4-6]. Therefore, it is still desirable to fabricate novel nanomaterials with high catalysis for developing advanced nitrite sensors.

Recently, MoS<sub>2</sub>, a graphene-like transition metal dichalcogenide, has received tremendous attention in electrochemical sensor due to its flexible structure, large surface area, active defects and amplified edge effects [7,8]. Usually, the composites of MoS<sub>2</sub> with other functional material such as conductive graphene, carbon nanotube or polymers and catalytic active metal or metal oxide nanoparticles are often used to overcome the intrinsic low conductivity and poor catalysis of primary MoS<sub>2</sub> for enhanced sensing performance [7,8]. At present, nitrite sensors based on MoS<sub>2</sub> hybrid with Fe<sub>3</sub>O<sub>4</sub> [9], Fe<sub>2</sub>O<sub>3</sub> [10], PrFeO<sub>3</sub> [11], PANI [12], AgNPs [13], MWCNT-Au have been reported [14]. However, these sensors still suffer from complex preparation, narrow linear responsive range, low sensitivity and high cost. Therefore, a new MoS<sub>2</sub> based hybrid with facile preparation, wide responsive range, high catalysis and low cost is still desirable for sensitive detection of nitrite.

Previous reports revealed that polyoxometalates (POMs) have good catalysis for nitrite reduction or oxidation [15,16], and its hybrid with carbon nanomaterial such as CNT [17], or rGO have been explored for nitrite sensing [18-21]. Compared with these carbon materials, MoS<sub>2</sub> has the advantage of easy preparation, flexible structures and plenty of active sites for functional material loading [7]. However, to the best of our knowledge, hybrid of MoS<sub>2</sub> with POMs for nitrite sensor has not been reported.

In this study, phosphomolybdic acid (PMA) was integrated with MoS<sub>2</sub> and reduced graphene oxide (rGO) to form a new ternary hybrid PMA-MoS<sub>2</sub>-rGO for nitrite sensing. The dual role of PMA as catalysis for nitrite oxidation and Mo source for MoS<sub>2</sub> growth makes the preparation of the hybrid can be achieved by one-pot hydrothermal reaction. Due to the synergy of these components, the hybrid PMA-MoS<sub>2</sub>-rGO with macroporous structure, large surface area and improved conductivity displayed greatly enhanced catalysis for the electrocatalytic oxidation of nitrite than those of MoS<sub>2</sub>, or PMA-MoS<sub>2</sub>. For nitrite sensing, the PMA-MoS<sub>2</sub>-rGO based sensor displayed a linear range of 0.5 μM to 8000 μM with a LOD of 0.2 μM (S/N=3), and satisfactory recovery for nitrite detection in real water samples.

## 2. EXPERIMENTAL

### 2.1 Chemicals and reagents

Phosphomolybdic acid (PMA), sodium nitrite (NaNO<sub>2</sub>), sodium molybdate and thiourea were supplied from Aladdin Chemical Reagent Co. Ltd. (Shanghai, China). Concentrated sulfuric acid was purchased from Sinopharm Chemical Reagent Co., Ltd (Shanghai, China). Diluted sulfuric acid (0.1 M) was used as electrolyte in this study. Ultrapure water purified by Millipore System was used for the preparation of nitrite or electrolyte solutions.

## 2.2 Preparation of 3D PMA-MoS<sub>2</sub>-rGO hybrid

Graphene oxide (GO) was prepared according to our previous approach [24].

The preparation of the PMA-MoS<sub>2</sub>-rGO hybrid can be done through a one-pot hydrothermal reaction. First, GO (30 mg) was dispersed into water (30 mL) by ultrasonic treatment for 30 min to obtain GO suspension. Then, phosphomolybdic acid (0.5657 g) was added into the GO suspension, followed by 40 ml H<sub>2</sub>O, and 0.2 g thiourea. The mixture was ultrasonicated for 10 mins and then transferred to an autoclave and reacted at 220 °C for 24 h. After that, the product with column shape was collected and washed by ultrapure water three times and finally lyophilized for 12 h to obtain the hybrid PMA-MoS<sub>2</sub>-rGO.

Similar approach was also used to prepare PMA-MoS<sub>2</sub> for comparison, except that no GO was added. MoS<sub>2</sub> was prepared in similar approach without introduction of GO and using sodium molybdate to replace PMA as Mo source.

## 2.3 Preparation of modified electrodes

To prepare the PMA-MoS<sub>2</sub>-rGO modified electrode, PMA-MoS<sub>2</sub>-rGO hybrid (1.5 mg) was dispersed into 1.0 mL water under ultrasonication. Next, 5 µL of the suspension and 5 µL of Nafion (0.1wt% in water) was subsequently cast onto a cleaned GCE and dried in air. Thus-obtained electrode was denoted as PMA-MoS<sub>2</sub>-rGO/GCE. MoS<sub>2</sub> or PMA-MoS<sub>2</sub> modified electrodes were also prepared as MoS<sub>2</sub>/GCE, or PMA-MoS<sub>2</sub>/GCE, respectively. Modified electrodes were stored at ambient conditions.

## 2.4 Characterization and electrochemical measurements

The structure, component and morphology of the material were investigated by Scanning electron microscope (SEM, S-3400 scanning electron microscope operated at 20 kV, Hitachi, Japan), energy disperse spectroscopy (EDS), and transmission microscope (JEM 2100, JEOL, Japan). Raman spectroscopy test was performed on an HR800 spectroscopy (Horiba JY, Japan) with He-Ne laser light with wavelength of 633 nm and laser power of 2 mW.

Electrochemical measurements were conducted with a computer-controlled CHI 760D electrochemical workstation (CH Instrument, Shanghai). Traditional three-electrode system was adapted including platinum wire (counter electrode), saturated calomel electrode (reference electrode) and PMA-MoS<sub>2</sub>-rGO or other modified GCE (working electrode in 0.1 M H<sub>2</sub>SO<sub>4</sub>). Electrochemical impedance spectroscopy (EIS) analysis was carried out with the same set using 0.1 M KCl containing 1 mM [Fe(CN)<sub>6</sub>]<sup>4-/3-</sup> as electrolyte. The frequency range is from 0.1 Hz to 10<sup>5</sup> Hz with a pulse amplitude of 5 mV.

# 3. RESULTS AND DISCUSSION

## 3.1. Preparation and characterization of PMA-MoS<sub>2</sub>-rGO

Hybrid of rGO with noble metal, POMs or other active material for nitrite sensing have been

reported [25-27]. However, few reports about  $\text{MoS}_2$  hybrid with POMs for nitrite sensing has been published. Here,  $\text{MoS}_2$  was integrated with PMA and rGO to form a three dimensional macroporous hybrid PMA- $\text{MoS}_2$ -rGO for nitrite detection. Fig. 1a-c present the morphological images of the  $\text{MoS}_2$ , PMA- $\text{MoS}_2$ , and PMA- $\text{MoS}_2$ -rGO. Fig. 1a shows the  $\text{MoS}_2$  prepared using molybdate and thiourea displays a typical flower-sphere morphology. In comparison, sheet or ridge-like  $\text{MoS}_2$  connects with each other to form a continuously wrinkled and porous structure when PMA was used as the Mo source. The morphology difference of  $\text{MoS}_2$  in Fig. 1a and Fig. 1b may be caused by the change of growth kinetics as different Mo sources was used. Nevertheless, it seems that both of  $\text{MoS}_2$  in Fig. 1a and  $\text{MoS}_2$  in Fig. 1b are built of same basic unit-crosslinked  $\text{MoS}_2$  sheets, indicating PMA can be used as Mo source for the synthesis of  $\text{MoS}_2$ . Fig. 1c shows flower-like  $\text{MoS}_2$  sphere are intertwined with wrinkled semi-transparent rGO sheet, forming a 3D porous structure. The morphology is different from that of Fig.1b, indicating the introduction of rGO can also change the growth process. EDS results revealed the hybrid in Fig. 1c was composed of C, O, Mo, S, and P, confirming the formation of PMA- $\text{MoS}_2$ -rGO hybrid.

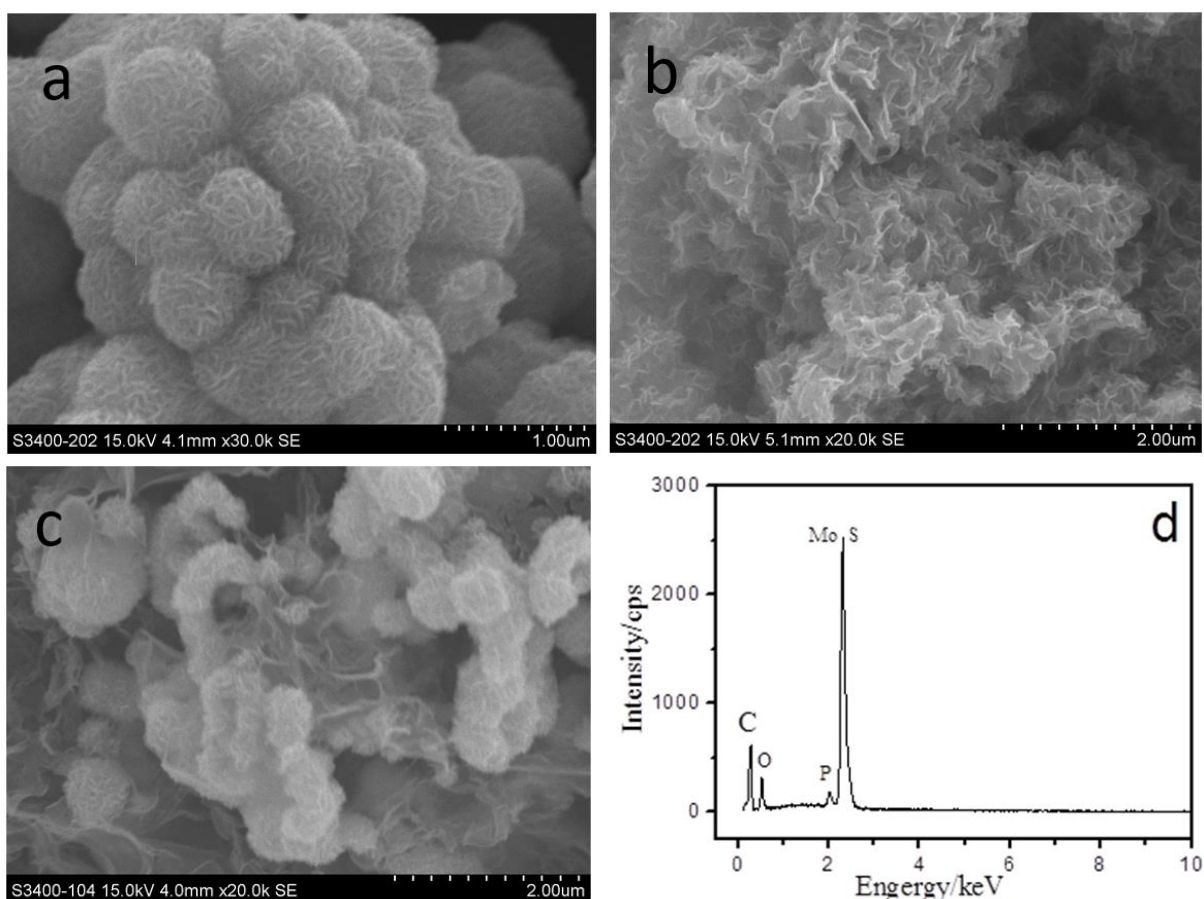


**Figure 1.** SEM images of  $\text{MoS}_2$  (a), (B) PMA- $\text{MoS}_2$  (b), PMA- $\text{MoS}_2$ -rGO hybrid (c) and (d) EDS results of the PMA- $\text{MoS}_2$ -rGO hybrid.

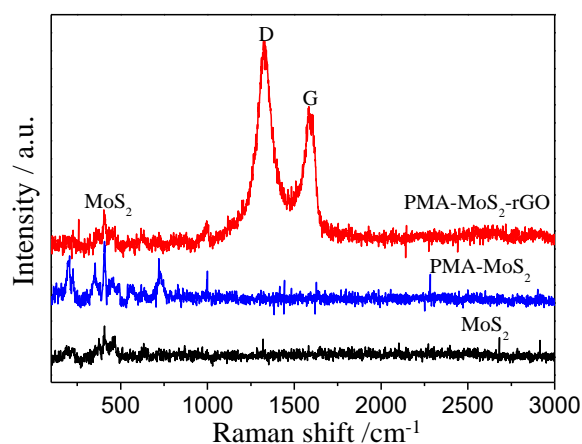


**Figure 2.** Raman spectram of MoS<sub>2</sub>, PMA-MoS<sub>2</sub>, and PMA-MoS<sub>2</sub>-rGO hybrid.

The structure of the hybrid also characterized by Raman spectroscopy. Fig.2 shows Raman spectra of MoS<sub>2</sub>, PMA-MoS<sub>2</sub>, and PMA-MoS<sub>2</sub>-rGO. The peak at 490 nm is found in all these three spectra, confirming the presence of MoS<sub>2</sub> [28]. Two dominant peaks at 1331 cm<sup>-1</sup> and 1603 cm<sup>-1</sup> were observed for PMA-MoS<sub>2</sub>-rGO, corresponding to the D band and G band of graphene. The  $I_D/I_G$  value increases from 1.14 for GO (not shown) to 1.47 for PMA-MoS<sub>2</sub>-rGO, indicating the significant reduction of GO during hydrothermal reaction [29]. The high  $I_D/I_G$  value of PMA-MoS<sub>2</sub>-rGO also indicating a strong interaction among PMA, MoS<sub>2</sub> and rGO, which introduces more actively defective sites on rGO plane [18].

These results from SEM, EDS, Raman spectrum and the electrochemical results in the next section confirmed that PMA-MoS<sub>2</sub>-rGO hybrid was successfully prepared.

### 3.2. Electrochemical characterization of PMA-MoS<sub>2</sub>-rGO hybrid

To learn about the electrochemical behavior of the hybrid, cyclic voltammetry and EIS measurement were first conducted. Fig. 3a shows the CVs of MoS<sub>2</sub>/GCE, PMA-MoS<sub>2</sub>/GCE, and PMA-MoS<sub>2</sub>-rGO/GCE in Fe(CN)<sub>6</sub><sup>3-/4-</sup> probe solution. Typical redox peaks of Fe(CN)<sub>6</sub><sup>3-/4-</sup> were found on all modified electrodes. Note, the peak currents response of Fe(CN)<sub>6</sub><sup>3-/4-</sup> on PMA-MoS<sub>2</sub>-rGO/GCE was larger than that obtained on MoS<sub>2</sub>/GCE or PMA-MoS<sub>2</sub>/GCE, indicating PMA-MoS<sub>2</sub>-rGO has the largest surface area. The large surface area of the hybrid can be ascribed to the intertwined structure of MoS<sub>2</sub> flower-sphere with rGO, which reduce the aggregation of rGO sheet and MoS<sub>2</sub> sphere, forming a 3D porous structure.

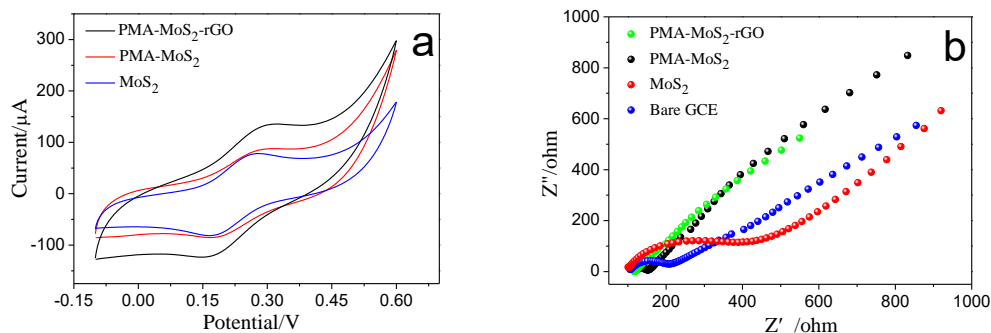


**Figure 3.** (a) CVs curves obtained from MoS<sub>2</sub>/GCE, PMA-MoS<sub>2</sub>/GCE, and PMA-MoS<sub>2</sub>-rGO/GCE in 0.5 mM K<sub>3</sub>Fe(CN)<sub>6</sub>; (b) EIS responses obtained from MoS<sub>2</sub>/GCE, PMA-MoS<sub>2</sub>/GCE, and PMA-MoS<sub>2</sub>-rGO/GCE in 0.1 M KCl-0.5 mM K<sub>3</sub>Fe(CN)<sub>6</sub>-K<sub>4</sub>Fe(CN)<sub>6</sub>. Pulse amplitude: 5 mV, Frequency: 0.1 Hz to 10<sup>5</sup> Hz;

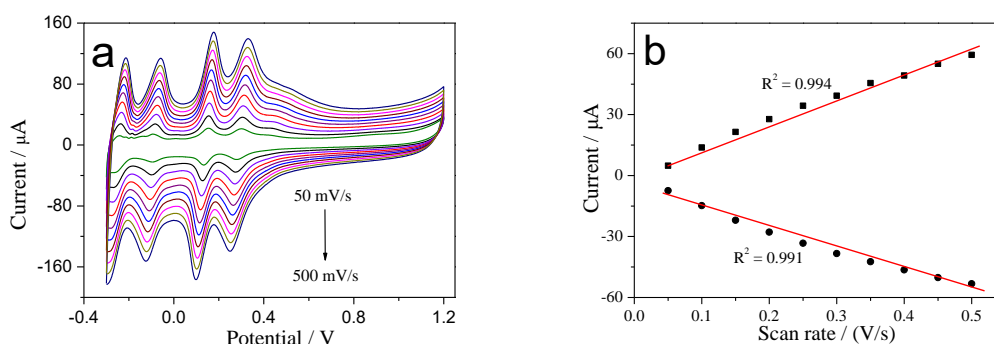


**Figure 4.** (a) CVs of PMA-MoS<sub>2</sub>-rGO/GCE at different scan rates in 0.1 M H<sub>2</sub>SO<sub>4</sub>. (b) calibration curves of redox peak currents at 0.1 V versus scan rate.

Electrochemical impedance spectrum was further employed to study the modified electrodes. Fig. 3b shows all the EIS curves of the modified electrodes display semi-circle patterns. The pattern of MoS<sub>2</sub>/GCE shows the largest diameter, implying MoS<sub>2</sub> prepared here has a large electron transfer resistance due to its intrinsic semiconductor property. The PMA-MoS<sub>2</sub>-rGO/GCE displays the smallest semicircle, demonstrating a good conductivity owing to the introduction of rGO as support. In addition, the slope of the straight-line part of the patterns from PMA-MoS<sub>2</sub>-rGO/GCE and PMA-MoS<sub>2</sub>/GCE are much higher than the GCE, indicating an improved mass transfer ability of the modified electrode due to their three-dimensional, open porous structures [30].

The electrochemical responses of the modified electrodes in diluted H<sub>2</sub>SO<sub>4</sub> at different scan rates were also studied. As shown in Fig. 4a, the characteristic redox peaks of PMA are clearly observed at all the spectrum, confirming the successful introduction of PMA in this hybrid. All peak currents steadily grow as scan rate increases. Well-defined characteristic peaks of PMA are still clearly distinguished at high scan rate, demonstrating fast electron transfer of the hybrid owing to the interlaced structure of rGO with MoS<sub>2</sub>. The peak current of PMA displays a linear dependence on the scan rate (Fig. 4b), demonstrating a surface adsorption-controlled process.

### 3.3. Electrocatalytic oxidation of nitrite

Nitrite salt can be detected by monitoring its reduction or oxidation current [31,32]. Previously, our work demonstrated that POM incorporated with 3D porous graphene was an efficient electrocatalyst for the oxidation of nitrite, and the proposed sensor could avoid the interference from dissolved oxygen [24]. The hybrid prepared here also presents 3D porous structure, and the PMA are stable confined in this 3D porous scaffold, thus a comparable or even better catalysis can be expected.

Here, the electrochemical response of these modified electrodes including MoS<sub>2</sub>/GCE, PMA-MoS<sub>2</sub>/GCE, and PMA-MoS<sub>2</sub>-rGO/GCE in the presence of nitrite were studied by cyclic voltammetry. Fig. 5a shows no apparent oxidation current can be found on the MoS<sub>2</sub>/GCE in the absence of nitrite. The current obviously increases at potential over 0.9 V when nitrite was added, forming a broad oxidation peak. These results imply MoS<sub>2</sub> is not an efficient catalysis for nitrite oxidation and thus incorporation of active species is necessary. For PMA-MoS<sub>2</sub>/GCE (Fig. 5b), no obvious redox peak of PMA can be found in the absence of nitrite.

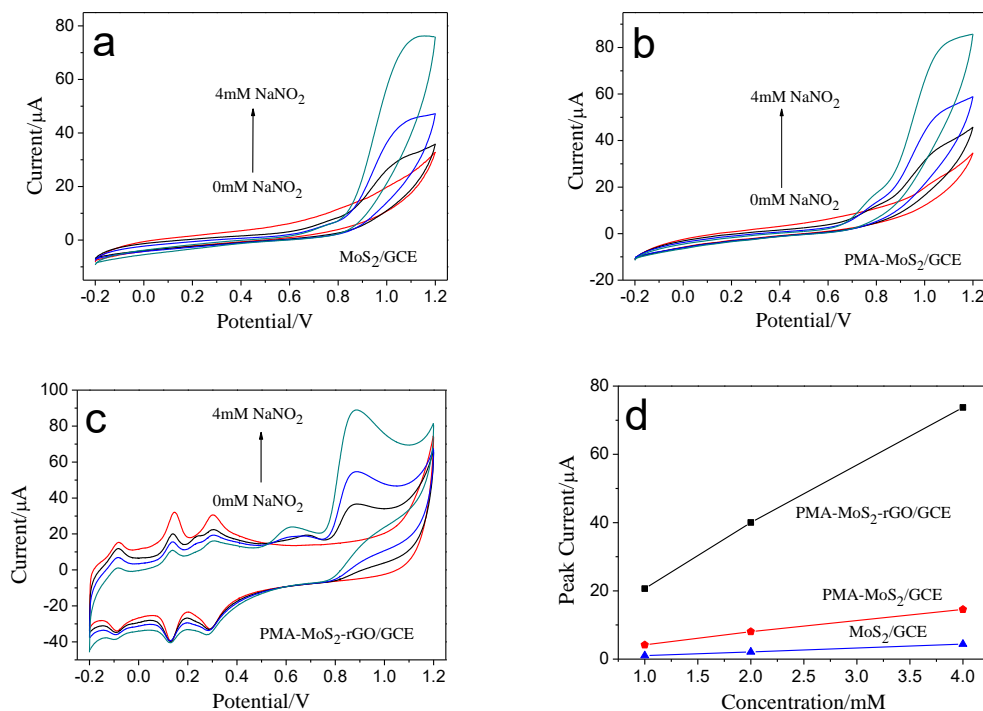


**Figure 5.** (a-c) CVs of 0-4 mM nitrite on (a) MoS<sub>2</sub>/GCE, (b) PMA-MoS<sub>2</sub>/GCE, and (c) PMA-MoS<sub>2</sub>-rGO/GCE. (d) Comparison of current response of nitrite on these modified electrodes.

The absence of redox peaks of PMA can be owing to the low conductivity of MoS<sub>2</sub>, which retards the electron transfer between different redox states of PMA. As nitrite was added, a weak oxidation peak at 0.8 V, and an obvious broad oxidation peak at 1.0-1.2V appear (Fig. 5b). The presence of the former weak peak indicates that PMA was participated in the nitrite oxidation. Nevertheless, the oxidation current likes that obtained on MoS<sub>2</sub>/GCE (Fig. 5a), implying a low activity. In Fig. 5c, three pairs of obvious redox peaks are found on PMA-MoS<sub>2</sub>-rGO/GCE in the absence of nitrite (red line in Fig. 5c).

These characteristic redox peaks of PMA with large current response not only confirm the incorporation of PMA in the hybrid [18,24], but also indicate that the hybrid with large surface area has good conductive network for electron transfer. The obvious redox peaks of PMA imply PMA can be efficiently utilized to catalyze the oxidation of nitrite. When nitrite was added, a weak oxidation peak at 0.67 V, and a large, significant oxidation peak at 0.87 V are found. The later oxidation peak is well-defined with much strong peak current. Fig. 5d clearly shows the oxidation peak currents of nitrite on PMA-MoS<sub>2</sub>-rGO/GCE are much higher than that obtained on MoS<sub>2</sub>/GCE, or PMA-MoS<sub>2</sub>/GCE. Importantly, the sensitivity for detection of nitrite in the range of 0-4 mM on PMA-MoS<sub>2</sub>-rGO/GCE are also much higher than those obtained on MoS<sub>2</sub>/GCE, or PMA-MoS<sub>2</sub>/GCE. All these results demonstrate that PMA-MoS<sub>2</sub>-rGO with 3D porous morphology, good conductivity, and integrated structure has greatly enhanced catalysis towards the oxidation of nitrite, which has great potential for highly sensitive detection of nitrite.

The improved catalysis observed on the hybrid PMA-MoS<sub>2</sub>-rGO can be attributed to the synergy among the component PMA, MoS<sub>2</sub> and rGO. The high electronegativity of metal-oxygen of PMA anchored onto graphene can induce more active sites, and thus improves its catalysis for nitrite oxidation [18]. Charge transfer from the PMA to graphene also contributed to the enhanced catalysis according to previous theoretical study [33]. Similar charge transfer may also take place between PMA and MoS<sub>2</sub>, which reduces the electron density of PMA and thus decrease its reducibility, or enhance its oxidation power [33]. When PMA is anchored onto the PMA-MoS<sub>2</sub>-rGO with porous structure, these effects are retained and possibly amplified as flowerlike MoS<sub>2</sub> could reduce the agglomeration of rGO nanosheet, and thus enlarged surface area is available to anchor POM, and consequently more active sites are exposed [20]. In sum, the integration of PMA, MoS<sub>2</sub> and rGO brought increased active sites, improved oxidation ability of PMA, facilitated electron transfer and improved mass transport of the sensing interface. The synergy among these factors result in a greatly enhanced catalysis of PMA-MoS<sub>2</sub>-rGO.

#### 3.4. Amperometric detection of nitrite

The hybrid PMA-MoS<sub>2</sub>-rGO with high catalysis for nitrite oxidation was used to construct a nonenzymatic nitrite sensor. Fig. 6a shows the current responses of the PMA-MoS<sub>2</sub>-rGO/GCE when different concentrations of nitrite were successively introduced into the solution. As can be seen, the amperometric current response at 0.87 V gradually increases as more nitrite was added.

The corresponding calibration curve indicates a linear dependence relationship was established between the current response and the concentration of nitrite in the ranges of 0.5  $\mu$ M to 8 mM (Fig. 6b). The detection limit is calculated to be 0.2  $\mu$ M (S/N=3). This performance is comparable or better than some previous nitrite sensors based on MoS<sub>2</sub>, rGO, POMs or noble metal as listed in Tab. 1 [18, 35-38].

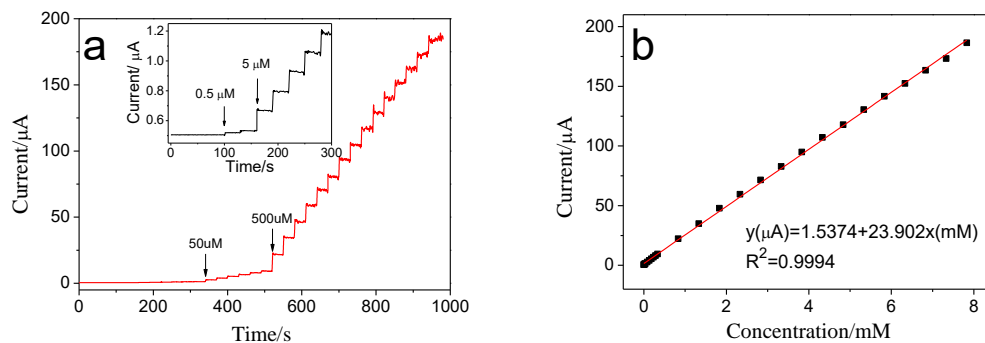


**Figure 6.** (a) Chronoamperometric response of PMA-MoS<sub>2</sub>-rGO/GCE for successive injection of nitrite in 0.1 M H<sub>2</sub>SO<sub>4</sub> at applied potential of 0.87 V. (b) The calibration curve of current response versus nitrite concentration.

**Table 1.** Analytical performances of some nitrite sensors.

Electrode material	Potential (V)	Linear range (μM)	Detection limit (μM)	Sensitivity (μA·mM <sup>-1</sup> ·cm <sup>-2</sup> )	Ref.
Fe <sub>3</sub> O <sub>4</sub> /MoS <sub>2</sub>	0.9	1-2630	0.5	15.28	[9]
Fe <sub>2</sub> O <sub>3</sub> /MoS <sub>2</sub>	1.0	2-6730	1.0	56.66	[10]
PANI-MoS <sub>2</sub>	0.9	4-4838	1.5	230.7	[12]
Ag-HNT-MoS <sub>2</sub>	0.8	2-245	0.7	2900	[13]
MoS <sub>2</sub> -MWCNT-Au	0.7	12-6500	4.0	41.61	[14]
rGO-POM	0.6	0-600	--	--	[18]
CR-GO	0.8	8.9-167	1	26.7	[34]
Pd/rGO	0.75	1-1000	0.23	298.1	[35]
PW <sub>12</sub> O <sub>40</sub> <sup>3-</sup>	-0.05	30-1000	28	15667	[36]
H <sub>3</sub> PMo <sub>12</sub> O <sub>40</sub> /PPy/gold	0.1	10-38000	4	258.8	[37]
Cu-NDs/RGO	-0.2	1.25-13000	0.4	214	[38]
PMA-MoS <sub>2</sub> /rGO	0.87	0.5-8000	0.2	379.4	This work

The wide linear responsive range, high sensitivity and low detection limit further confirm the advantage of the hybrid for nitrite detection.

### 3.5. Selectivity, reproducibility and stability

To evaluate the selectivity of the PMA-MoS<sub>2</sub>-rGO based sensor, the current response of the

sensor for nitrite in the presence of other possible interferences was recorded. As can be seen in Fig. 7, those coexisted materials including nitrate and other inorganic salts, small organic molecules glucose or uric acid, and metal ions do not interfere the current response of nitrite at 0.87 V on PMA-MoS<sub>2</sub>-rGO/GCE, indicating the sensor has a good selectivity.

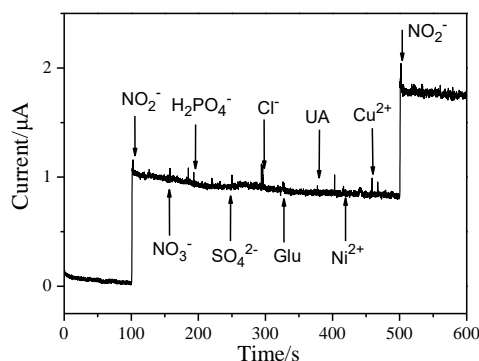


**Figure 7.** Amperometric response for nitrite and coexisting substances on PMA-MoS<sub>2</sub>-rGO/GCE at applied potential of 0.87 V. The concentrations of these substances are 50 µM.

The reproducibility of the sensor was evaluated by recording the current response for repeated analyte injection and parallel-prepared electrodes. The RSD of current response of nitrite on PMA-MoS<sub>2</sub>-rGO/GCE is 3.5% for five-time successive measurements at 0.2 mM concentration, and the value is 5.1% for five independent prepared electrodes. After storage the PMA-MoS<sub>2</sub>-rGO/GCE in air for one month, over 90% percent of original current response value retained, indicating a good stability. The improved stability of this PMA-MoS<sub>2</sub>-rGO can be ascribed to the strong interactions between GO and PMA like that reported in reference [18], and the integrated structure obtained from the one-pot hydrothermal treatment.

### 3.6. Real sample analysis

**Table 2.** Determination of nitrite in water sample.

Sample	Original (µM)	Added (µM)	Found (µM)	RSD (%)	Recovery (%)
1	--	10.00	10.12	3.7	101.2
2	2.46	20.00	23.12	2.9	102.9
3	3.52	30.00	33.71	4.1	100.6
4	5.61	50.00	55.32	4.7	99.5

According to the World Health Organization (WHO), the guidance level for short-term exposure

for nitrite ions and a provisional guidance level for long-term exposure for nitrite ions is 65  $\mu\text{M}$  and 4.3  $\mu\text{M}$ , respectively [39]. The above section proved that the detection limit from the PMA-MoS<sub>2</sub>-rGO/GCE is well below the guide level. Thus, the practical application of the sensor for nitrite detection in water sample was investigated in this section. Water samples from local lake are filtered and doped with diluted H<sub>2</sub>SO<sub>4</sub> as supporting electrolyte, and other operations followed the standard procedure. As can be seen in Table 2.

The results show the present method displays a recovery among 99.5% to 102.9% for nitrite sensing in water sample, indicating a great potential of the developed sensor in monitoring nitrite level in water analysis and environmental samples.

#### 4. CONCLUSIONS

In this study, a new hybrid of PMA-MoS<sub>2</sub>-rGO with porous structure has been prepared by one-pot hydrothermal reaction for nitrite detection. Our results revealed PMA played a dual role including as Mo source for the growth of flower-sphere-like MoS<sub>2</sub>, and as active catalysis for electrochemical oxidation of nitrite. Owing to the 3D porous structure and the synergy among these components, the PMA-MoS<sub>2</sub>-rGO displayed much enhanced catalysis for nitrite oxidation. A nonenzymatic sensor for nitrite was successfully fabricated, which displayed a wide linear responsive range of 0.5  $\mu\text{M}$  to 8000  $\mu\text{M}$ , and a low detection limit of 0.2  $\mu\text{M}$ . The proposed sensor also showed good selectivity, high stability, and satisfactory recovery for real sample analysis. Similar approach can be used to prepare other MoS<sub>2</sub> based hybrid [40], and these hybrids with simple preparation, high catalytic activity and good stability hold great potential in environmental monitoring, chemical sensors and so on.

#### CONFLICTS OF INTEREST

There are no conflicts to declare.

#### ACKNOWLEDGEMENT

This work is financially supported by the National Natural Science Foundation of China (21665011, 21705063), Natural Science Foundation of Jiangxi Province (20161BAB203088).

#### References

1. J.K.S. Moller, and L.H. Skibsted, *Chem. Rev.*, 102 (2002) 1167.
2. N. Hui, F.L. Chai, P.P. Lin, Z.L. Song, X.T. Sun, Y.N. Li, S.Y. Niu, and X.L. Luo, *Electrochim. Acta*, 199 (2016) 234.
3. D. Liu, Q.H. Guo, X.P. Zhang, H.Q. Hou, and T.Y. You, *J. Colloid Interface Sci.*, 450 (2015) 168.
4. M. Zhang, J. Zheng, J.P. Wang, J.L. Xu, T. Hayat, and N.S. Alharbi, *Sens. Actuators B- Chem.*, 282 (2019) 85.
5. J. Yang, L.T. Yang, H.L. Ye, F.Q. Zhao, and B.Z. Zeng, *Electrochim. Acta*, 219 (2016) 647.
6. W.L. Sun, S. Zhang, H.Z. Liu, L.T. Jin, and J.L. Kong, *Anal. Chim. Acta*, 388 (1999) 103.
7. A. Sinha, Dhanjai, B. Tan, Y.J. Huang, H.M. Zhao, X.M. Dang, J.P. Chen, and R. Jain, *Trends Anal. Chem.*, 102 (2018) 75.

8. A.T. Ezhil Vilian, B. Dinesh, S.M. Kang, U.M. Krishnan, Y.S. Huh, and Y.K. Han, *Microchim. Acta*, 186 (2019) 203.
9. Y. Zhang, P. Chen, F. Wen, B. Yuan, and H. Wang, *J. Electroanal. Chem.*, 761 (2016) 14.
10. H. Wang, P. Chen, F. Wen, Y. Zhu, and Y. Zhang, *Sens. Actuators B-Chem.*, 220 (2015) 749.
11. H. Huang, L. Lv, F. Xu, J. Liao, S. Liu, and H. Wen, *Microchim. Acta*, 184 (2017) 4141.
12. Y. Zhang, P. Chen, F. Wen, C. Huang, and H. Wang, *Ionics*, 22 (2016) 1095.
13. M. Ghanei-Motlagh, and M.A. Taher, *Biosens. Bioelectron.*, 109 (2018) 279.
14. Y. Zhang, F. Wen, J. Tan, C. Jiang, M. Zhu, Y. Chen, and H. Wang, *J. Electroanal. Chem.*, 786 (2017) 43.
15. Q.W. Wang, J. Khungwa, L. Li, Y. Liu, X.H. Wang, and S.T. Wang, *J. Electroanal. Chem.*, 824 (2018) 91.
16. Y.C. Ji, L.J. Huang, J. Hu, C. Streb, and Y.F. Song, *Energy Environ. Sci.*, 3 (2015) 776.
17. Q.Y. Tang, X.X. Luo, and R.M. Wen, *Anal. Lett.*, 38 (2005) 1445.
18. Y. Kim, and S. Shanmugam, *ACS Appl. Mater. Interfaces*, 5 (2013) 12197.
19. Z.Y. Bai, C.L. Zhou, H.B. Xu, G.N. Wang, H.J. Pang, and H.Y. Ma, *Sens. Actuators B-Chem.*, 243 (2017) 361.
20. G.R. Ma, M. Yang, F.G. Xu, and L. Wang, *Anal. Methods*, 9 (2017) 5140.
21. G.R. Ma, H. Xu, F.G. Xu, and L. Wang, *Int. J. Electrochem. Sci.*, 12 (2017) 7365.
22. C.P. Gu, W.M. Guan, Y.W. Cui, Y. Chen, L.L. Gao, and J.R. Huang, *J. Mater. Chem. A*, 4 (2016) 17000.
23. X.J. Zhao, X.H. Xia, S.J. Yu, and C.M. Wang, *Anal. Methods*, 6 (2014) 9375.
24. G.R. Ma, M. Yang, G.C. Zhao, Y.P. Zhang, F.G. Xu, and L. Wang, *Anal. Methods*, 8 (2016) 7405.
25. D. Zhang, H.Y. Ma, Y.Y. Chen, H.J. Pang, and Y. Yu, *Anal. Chim. Acta*, 792 (2013) 35.
26. S.M. Choi, M.H. Seo, H.J. Kim, E.J. Lim, and W.B. Kim, *Int. J. Hydrogen Energy*, 13 (2010) 6853.
27. W.H. Guo, X.H. Cao, Y.H. Liu, X.L. Tong, and X.S. Qu, *J. Electrochem. Soc.*, 161 (2014) B248.
28. K. Pramoda, K. Moses, U. Maitra, and C.N.R. Rao, *Electroanalysis*, 27 (2015) 1892.
29. F.G. Xu, M. Deng, G.Y. Li, S.H. Chen, and L. Wang, *Electrochim. Acta*, 88 (2013) 59.
30. F.G. Xu, Y. Liu, G.H. Ding, M. Deng, S.H. Chen, and L. Wang, *Electrochim. Acta*, 150 (2014) 223.
31. F.G. Xu, M. Deng, Y. Liu, X.C. Ling, X.Y. Deng, and L. Wang, *Electrochem. Commun.*, 47 (2014) 33.
32. J.H. Yuan, X.L. Jin, N. Li, J.R. Chen, J.G. Miao, Q.X. Zhang, L. Niu, and J.X. Song, *Electrochim. Acta*, 56 (2011) 10069.
33. S. Wen, W. Guan, J. Wang, Z. Lang, L. Yan, and Z. Su, *Dalton Trans.*, 41 (2012) 4602.
34. V. Mani, A.P. Periasamy, and S.M. Chen, *Electrochem. Commun.*, 17 (2012) 75.
35. L. Fu, S. Yu, L. Thompson, and A. Yu, *RSC Adv.*, 5 (2015) 40111.
36. R. Ojani, M.S. Rahmanifar, and P. Naderi, *Electroanalysis*, 20 (2008) 1092.
37. Q.Y. Tang, X.X. Luo, and R.M. Wen, *Anal. Lett.*, 38 (2005) 1445.
38. D. Zhang, Y.X. Fang, Z.Y. Miao, M. Ma, X. Du, S. Takahashi, J.I. Anzaib, and Q. Chen, *Electrochim. Acta*, 107 (2013) 656.
39. M. Khairy, R.O. Kadara, and C.E. Banks, *Anal. Methods*, 2 (2010) 851.
40. J.P. Wang, M. Zhang, T. Miao, Y. Ling, Q. Wen, J. Zheng, J.L. Xu, T. Hayat and N.S. Alharbid, *Inorg. Chem. Front.*, 5 (2018) 844.